European Journal of Medicinal Chemistry 47 (2012) 312–322

Contents lists available at SciVerse ScienceDirect

European Journal of Medicinal Chemistry

journal homepage: http://www.elsevier.com/locate/ejmech

Original article

# Synthesis and QSAR study of novel cytotoxic spiro[3*H*-indole-3,2′(1′*H*)-pyrrolo[3,4-*c*]pyrrole]-2,3′,5′(1*H*,2′*aH*,4′*H*)-triones

Adel S. Girgis [a,*], Jacek Stawinski [b,**], Nasser S.M. Ismail [c], Hanaa Farag [a]

[a] *Pesticide Chemistry Department, National Research Centre, Dokki, Cairo 12622, Egypt*
[b] *Department of Organic Chemistry, Arrhenius Laboratory, Stockholm University, S-106 91 Stockholm, Sweden*
[c] *Pharmaceutical Chemistry Department, Faculty of Pharmacy, Ain Shams University, Cairo, Egypt*

ARTICLE INFO

*Article history:*
Received 5 August 2011
Received in revised form
27 October 2011
Accepted 28 October 2011
Available online 7 November 2011

*Keywords:*
1*H*-pyrrole-2,5-diones
Azomethine ylides
Spiro[3*H*-indole-3,2′(1′*H*)-pyrrolo[3,4-*c*]pyrrole]
Anti-tumor
QSAR

ABSTRACT

1,3-Dipolar cycloaddition reaction of 1-aryl-1*H*-pyrrole-2,5-diones **1a-e** with non-stabilized azomethine ylides, generated in situ via decarboxylative condensation of isatins **2a**–**c** and sarcosine (**3**) in refluxing ethanol, afforded 4′-aryl-5′*a*,6′-dihydro-1′-methyl-spiro[3*H*-indole-3,2′(1′*H*)-pyrrolo[3,4-*c*]pyrrole]-2,3′,5′(1*H*,2′*aH*,4′*H*)-triones **4a**–**o** in good yields. Compound **4l** exhibited high anti-tumor activity against HEPG2 (liver cancer) cell line ($IC_{50} = 12.16$ μM) compared to that of Doxorubicin ($IC_{50} = 7.36$ μM), and the other synthesized compounds revealed moderate anti-tumor properties against HCT116 (colon), MCF7 (breast) and HEPG2 (liver) human tumor cell lines. 3D-Pharmacophore modeling and quantitative structure-activity relationship (QSAR) analysis were combined to explore the structural requirements controlling the observed anti-tumor properties. It was found that the major structural factors affecting potency of these compounds were related to their basic skeleton.



## 1. Introduction

In the last few decades increasing interest has been directed towards construction of spiropyrrolidinyl-oxindole containing compounds [1]. This could be attributed to the fact that many spiropyrrolidinyl-oxindolyl analogues have been isolated from natural sources and identified as promising bio-active agents, e.g., spirotryprostatine A and spirotryprostatine B that were found to be inhibitors of mammalian cell cycle at G2/M phase, from the secondary metabolites of *Aspergillus fugimatus* [2,3]. Elacomine [4] was isolated from *Eleagnus commutata*, and horsfiline [5–10], from *Horsfieldia superba*, a small Malaysian tree, extracts of which have found use in indigenous medicine. Mitraphylline was isolated from *Uncaria tomentosa* (cat's claw) and identified as anti-tumor active agent against human brain cancer cell lines, neuroblastoma SKN-BE(2), and malignant glioma GAMG [11]. Generally, several oxindole derivatives are well known as anti-tumor active agents due to their kinase inhibitory properties [12–16], especially, tyrosine kinase [12–14].

In the present work, we intended to investigate synthesis of spiro[3*H*-indole-3,2′(1′*H*)-pyrrolo[3,4-*c*]pyrrole]-2,3′,5′(1*H*,2′*aH*,4′*H*)-triones by utilizing 1,3-dipolar cycloaddition of 1-aryl-1*H*-pyrrole-2,5-dione derivatives with non-stabilized azomethine ylides generated in situ via decarboxylative condensation of isatins with α-amino acids according to the previously described procedure [17], and to evaluate their anti-tumor properties against a variety of human tumor cell lines (HCT116 "colon", MCF7 "breast" and HEPG2 "liver" cancers). One of the driving forces for initiating this work was our previous observation that compounds with alkaloid heterocyclic system skeletons, such as dispiro[1*H*-indene-2,3′-pyrrolidine-2′,3″-[3*H*]indole]-1,2″(1″*H*)-diones and dispiro[3*H*-indole-3,2′-pyrrolidine-3′,3″-piperidine]-2(1*H*),4″-diones, revealed promising anti-tumor properties against SK-MEL-2 (melanoma) cell line [18], and colon (HCT-116), breast (T-47D), leukemia [HL-60 (TB), MOLT-4, RPMI-8226] and prostate (PC-3) cell line cancers [19]. In this work, quantitative structure-activity relationship (QSAR) studies were also performed, not only for validating the observed pharmacological properties but also, for investigating the most important parameters controlling these properties.

## 2. Results and discussion

### 2.1. Chemistry

Reaction of 1-aryl-1*H*-pyrrole-2,5-diones **1a**–**e** with non-stabilized azomethine ylides, generated in situ via decarboxylative

* Corresponding author. Tel.: +20 2 01220447199; fax: +20 2 33370931.
** Corresponding author. Fax: +46 8 15 49 08.
*E-mail addresses:* girgisas10@yahoo.com (A.S. Girgis), js@organ.su.se (J. Stawinski).

0223-5234/$ – see front matter © 2011 Elsevier Masson SAS. All rights reserved.
doi:10.1016/j.ejmech.2011.10.058

condensation of isatins **2a**–**c** and sarcosine (**3**) as a representative example of α-amino acid, afforded in refluxing ethanol only one product as indicated by TLC analysis.The structures of the isolated compounds were established to be 4′-aryl-5′*a*,6′-dihydro-1′-methyl-spiro[3*H*-indole-3,2′(1′*H*)-pyrrolo[3,4-*c*]pyrrole]-2,3′,5′(1*H*,2′*aH*,4′*H*)-triones **4a**–**o** (Scheme 1) based on spectroscopic (IR, $^1$H NMR, $^{13}$C NMR, $^1$H,$^1$H-COSY, HSQC, MS) and elemental analyses data. $^1$H NMR spectrum of **4a**, as a representative example of the synthesized compounds, reveals the presence of four signal sets, due to the diastereotopic methylene protons $H_2$C-6′ at $\delta = 3.36$, 3.63 ppm, and two methine protons, *H*-2′*a* and *H*-5′*a*, at $\delta = 3.55$, 3.75 ppm, respectively. $^1$H,$^1$H-COSY spectrum of compound **4a** supports these interpretations. $^{13}$C NMR (on-resonance) spectrum of **4a** exhibits the methylene ($H_2C$-6′) and methine (HC-5′*a*, HC-2′*a*) carbons at $\delta = 54.1$, 44.6 and 52.0 ppm, respectively. A signal from the quaternary spiro-carbon, "*C*-3 (*C*-2′)", appears at $\delta = 72.2$ ppm, and those from the carbonyl carbons, at $\delta = 174.0$, 177.8 and 178.1 ppm $^1$H,$^{13}$C-heteronuclear single quantum coherence (HSQC) spectrum of compound **4a** supports these assignments (Fig. 1). The other synthesized analogues revealed similar spectral features (*c.f.* experimental section). The structural assignments for the synthesised compounds have been substantiated by mass spectral data (EI-MS) that reveal the corresponding parent ion peaks as either base peaks or high relative intensity signals.

Single crystal X-ray studies of **4a** and **4m** add a conclusive support for the assigned structures. They reveal that both the pyrrolidinyl nuclei appear as typical five-membered heterocycles (pentagonal structure) where, each of them seems like an opened-envelope and fused together with angles C(12)–C(10)–C(21) = 113.5(1), C(7)–C(14)–C(11) = 112.4(1)° (in case of compound **4a**) and C(14)–C(17)-C(26) = 111.6(2), C(13)–C(23)–C(15) = 114.3(2)° (in case of compound **4m**). The methine protons (*H*-2′*a*, *H*-5′*a*) were observed in *cis*-configuration [C(12)–C(10)–H(10) = 111.3(1), C(14)–C(10)–H(10) = 109.4(1), C(21)–C(10)–H(10) = 111.6(1), C(7)–C(14)–H(14) = 112.0(2), C(10)–C(14)–H(14) = 109.5(1), C(11)–C(14)–H(14) = 112.4(2)° (in case of compound **4a**) and C(14)–C(17)–H(17) = 113.1(2), C(23)–C(17)–H(17) = 109.4(2), C(26)–C(17)–H(17) = 112.3(2), C(13)–C(23)-H(23) = 109.0(2), C(15)–C(23)-H(23) = 109.0(2), C(17)–C(23)–H(23) = 114.5(2)° (in case of compound **4m**)]. The 2-oxindole ring appears as a nearly planar system linked with the fused pyrrolo[3,4-*c*]pyrrol residue through the spiro-carbon connection, "*C*-3 (*C*-2′)", (Figs. 2 and 3).

Theoretical calculations using both AM1 and PM3 methods were carried out to compare the observed geometric parameters obtained from single crystal X-ray analysis with the calculated ones (Table 1 of supplementary material). Geometries of compounds **4a** and **4m**

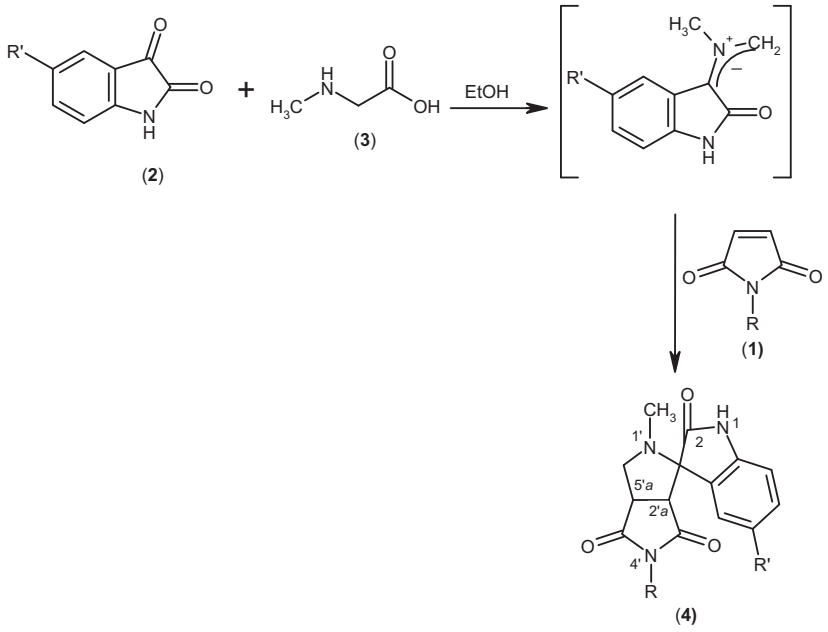


**1a**, R = Ph
**1b**, R = 4-Cl$C_6H_4$
**1c**, R = 4-F$C_6H_4$
**1d**, R = 4-$H_3CC_6H_4$
**1e**, R = 4-$H_3COC_6H_4$

**2a**, R' = H
**2b**, R' = Cl
**2c**, R' = $OCH_3$

**4a**; R = Ph, R' = H
**4b**; R = Ph, R' = Cl
**4c**; R = Ph, R' = $OCH_3$
**4d**; R = 4-Cl$C_6H_4$, R' = H
**4e**; R = 4-Cl$C_6H_4$, R' = Cl
**4f**; R = 4-Cl$C_6H_4$, R' = $OCH_3$
**4g**; R = 4-F$C_6H_4$, R' = H
**4h**; R = 4-F$C_6H_4$, R' = Cl
**4i**; R = 4-F$C_6H_4$, R' = $OCH_3$
**4j**; R = 4-$H_3CC_6H_4$, R' = H
**4k**; R = 4-$H_3CC_6H_4$, R' = Cl
**4l**; R = 4-$H_3CC_6H_4$, R' = $OCH_3$
**4m**; R = 4-$H_3COC_6H_4$, R' = H
**4n**; R = 4-$H_3COC_6H_4$, R' = Cl
**4o**; R = 4-$H_3COC_6H_4$, R' = $OCH_3$

**Scheme 1.** Synthetic route of compounds **4a**–**o**.

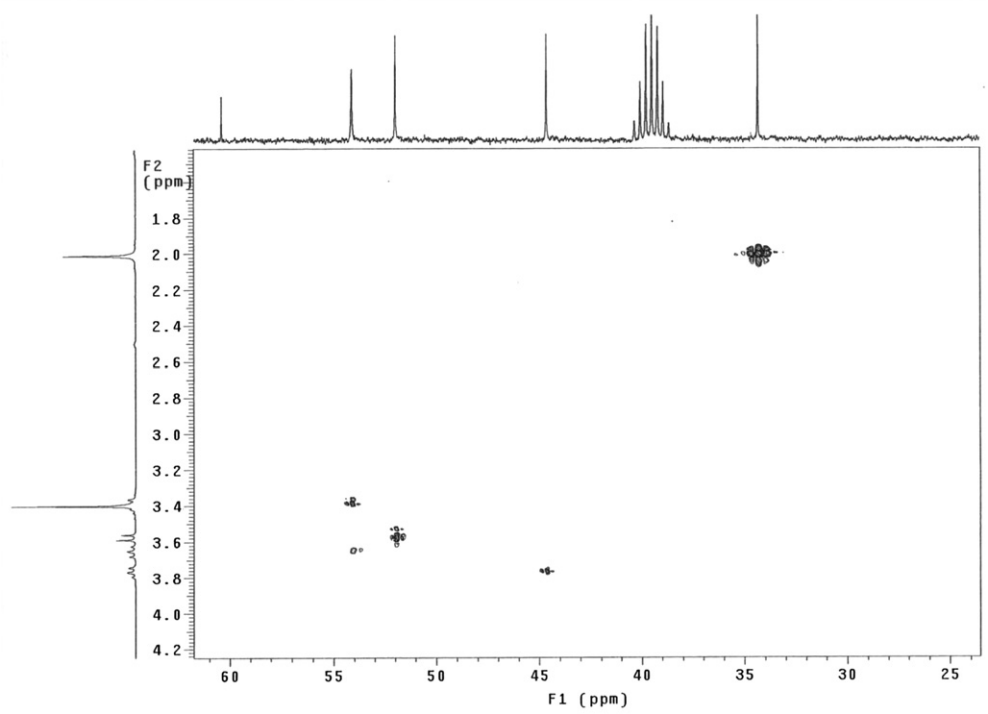


**Fig. 1.** $^{1}H$, $^{13}C$-Heteronuclear single quantum coherence (HSQC) spectrum of **4a**.

were optimized by the molecular mechanics force field (MM+), followed by either semi-empirical AM1 [20] or PM3 [21,22] methods implemented in the HyperChem 8.0 package. The structures were fully optimized without fixing any parameters, thus bringing all geometric variables to their equilibrium values. The energy minimization protocol employed the Polak–Ribiere conjugated gradient algorithm. Convergence to a local minimum was achieved when the energy gradient was $\leq$0.01 kcal mol$^{-1}$. The RHF method was used in the spin pairing for the two semi-empirical tools [23–25].

### 2.2. Anti-tumor properties

The synthesized compounds **4a-o** were screened for their anti-tumor properties against HCT116 (colon), MCF7 (breast) and HEPG2 (liver) human tumor cell lines utilizing the Sulfo-Rhodamine-B (SRB) standard method [26]. From the observed results (Table 1, Figs. 1–3 of supplementary material), it has been concluded that most of the synthesized compounds had moderate anti-tumor properties against the investigated human tumor cell lines. In contrast, compound **4l** exhibited considerable anti-tumor activity against HEPG2 (liver cancer) cell line with potency ($IC_{50}$ = 12.16 μM; concentration required to produce 50% inhibition of cell growth compared to control experimental) comparable to that of Doxorubicin ($IC_{50}$ = 7.36 μM), that was used as a reference standard during this study. In order to understand the observed pharmacological properties, quantitative structure-activity relationship (QSAR) study was initiated.

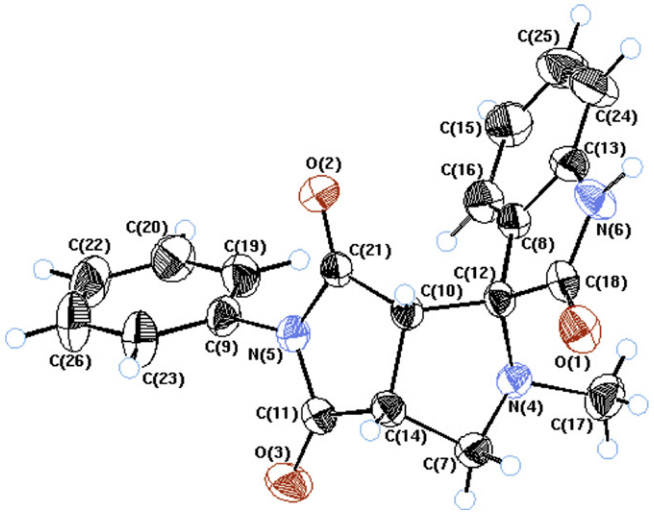


**Fig. 2.** ORTEP projection of single crystal X-ray diffraction of **4a**.

### 2.3. QSAR study

#### 2.3.1. 3D-QSAR pharmacophore modeling

This study was performed using Discovery Studio 2.5 software (Accelrys Inc., San Diego, CA, USA), which permits pharmacophore generation, structural alignment, activity prediction and 3D database creation [27–29]. 3D-QSAR pharmacophore protocol was used to generate predictive pharmacophores via aligning different conformations in which the molecules are likely to bind with the receptor. A given hypothesis could be combined with a known activity data to create a 3D-QSAR model that identifies overall aspects of molecular structure governing activity. 3D-QSAR based on pharmacophore was constructed using collections of molecules with activities ranging over a number of orders of magnitude. Pharmacophores explain the variability of bioactivity with respect to the geometric localization of the chemical features present in the molecules. The observed HYPOGEN identifies a 3D array of a maximum of four chemical features common to the training set **4a–f,h–k,m–o** that provides relative alignment for each input molecule, consistent with its binding mode to a proposed common receptor site. The chemical features considered were: hydrogen bond donor (HBD), hydrogen bond acceptor (HBA), hydrophobic (H) and positive ionizable features (PosIon) (Fig. 4, Table 2 exhibits

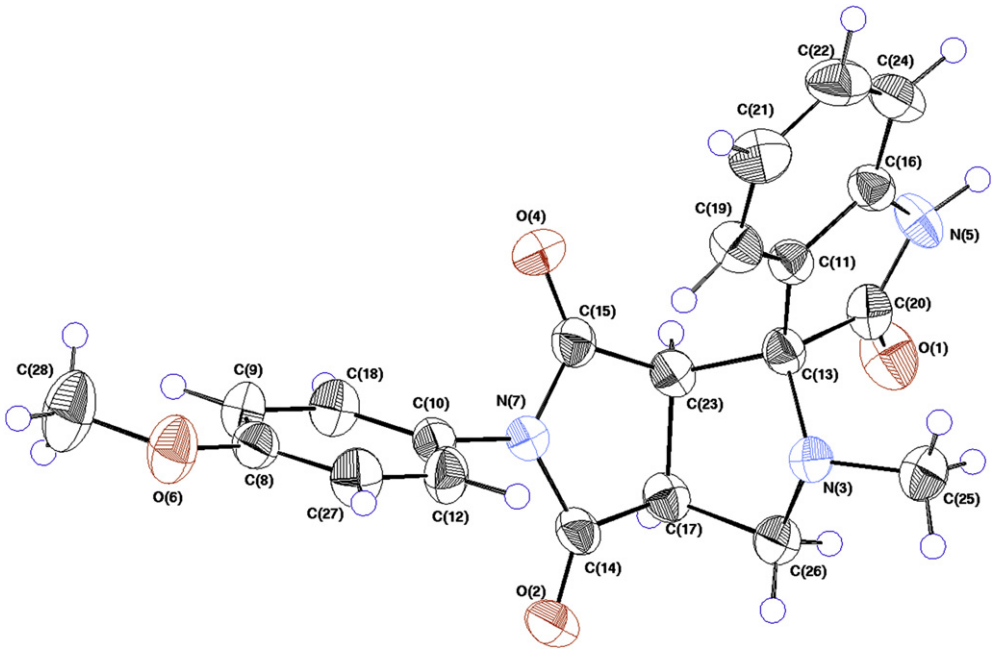


**Fig. 3.** ORTEP projection of single crystal X-ray diffraction of **4m**.

constraint distances and angles between features of the generated pharmacophores, Tables 3–5 exhibit fit values and estimated activities of the training set due to the generated 3D-pharmacophore models). The conformational flexibility of the training set was modelled by creating multiple conformers that covered a specified energy range for each input molecule [28,30,31]. Through the pharmacophore mapping study, it was found that the major structural factors affecting the potency of these compounds were related to their basic skeleton. In case of HCT116 (colon cancer) cell line pharmacophore model, the controlling features were two hydrogen bond acceptor sites together with a positive charged site, while for MCF7 (breast cancer) cell line, a hydrogen bond donor and a positive ionizable. On the other hand, both a hydrogen bond donor and an acceptor were required for the generated pharmacophore due to HEPG2 (liver cancer) cell line. In addition, hydrophobic features were recognized in all the generated 3D-pharmacophore models of the tested cancer types. Comparison of 3D-pharmacophore models generated for HCT116 (colon) and MCF7 (breast) cancers revealed that common pharmacophoric features recognized are the positive ionizable and hydrophobics with root mean square division (RMSD) value of 0.058. However, in case of HCT116 (colon) and HEPG2 (liver) cancers, the hydrogen bond acceptor and hydrophobics are the common features between them (RMSD = 0.334). For tumor lines MCF7 (breast) and HEPG2 (liver), the common pharmacophoric features were hydrogen bond donor and hydrophobics (RMSD = 0.329) (Fig. 4D–F). Mapping of the training set analogues into the generated 3D-QSAR pharmacophore based model is shown in Figs. 4–6 of the supplementary material.

### 2.3.2. QSAR modeling

Despite of the significance of pharmacophoric hypotheses for understanding ligand molecule affinity and 3D search queries, their predictive value as 3D-QSAR models is generally limited by steric shielding and bioactivity-modulating auxiliary groups (electron-donating or withdrawing functionalities) [32–34]. Thus, a classical

**Table 1**
Anti-tumor properties of the synthesized compounds.

| Entry | Compd. | R | R′ | $IC_{50}$, μg/ml (μM) | | |
|---|---|---|---|---|---|---|
| | | | | Colon cancer (HCT116) | Breast cancer (MCF7) | Liver cancer (HEPG2) |
| 1 | **4a** | Ph | H | 22.14 (63.73) | 12.38 (35.64) | 11.43 (32.90) |
| 2 | **4b** | Ph | Cl | 12.62 (33.05) | 14.76 (38.66) | 12.62 (33.05) |
| 3 | **4c** | Ph | $OCH_3$ | 12.86 (34.08) | 16.90 (44.78) | 16.67 (44.17) |
| 4 | **4d** | 4-$ClC_6H_4$ | H | 14.05 (36.80) | 16.43 (43.03) | 12.38 (32.42) |
| 5 | **4e** | 4-$ClC_6H_4$ | Cl | 14.76 (35.46) | 16.90 (40.60) | 12.14 (29.16) |
| 6 | **4f** | 4-$ClC_6H_4$ | $OCH_3$ | 19.52 (47.40) | 15.95 (38.73) | 17.86 (43.37) |
| 7 | **4g** | 4-$FC_6H_4$ | H | 15.48 (42.37) | 12.38 (33.88) | 31.90 (87.31) |
| 8 | **4h** | 4-$FC_6H_4$ | Cl | 29.29 (73.26) | 35.95 (89.92) | 16.43 (41.09) |
| 9 | **4i** | 4-$FC_6H_4$ | $OCH_3$ | 12.38 (31.31) | 17.38 (43.96) | 10.95 (27.69) |
| 10 | **4j** | 4-$H_3CC_6H_4$ | H | 16.67 (46.13) | 13.57 (37.55) | 27.86 (77.09) |
| 11 | **4k** | 4-$H_3CC_6H_4$ | Cl | >50.00 (>126.31) | 19.76 (49.92) | 25.00 (63.16) |
| 12 | **4l** | 4-$H_3CC_6H_4$ | $OCH_3$ | 18.10 (46.24) | 18.33 (46.83) | 4.76 (12.16) |
| 13 | **4m** | 4-$H_3COC_6H_4$ | H | 20.24 (53.63) | 18.10 (47.96) | 27.38 (72.55) |
| 14 | **4n** | 4-$H_3COC_6H_4$ | Cl | 16.90 (41.03) | 15.71 (38.14) | 11.90 (28.89) |
| 15 | **4o** | 4-$H_3COC_6H_4$ | $OCH_3$ | 16.67 (40.92) | 17.38 (42.66) | 20.24 (49.68) |
| 16 | Doxorubicin | – | – | 3.73 (6.86) | 2.97 (5.46) | 4.00 (7.36) |

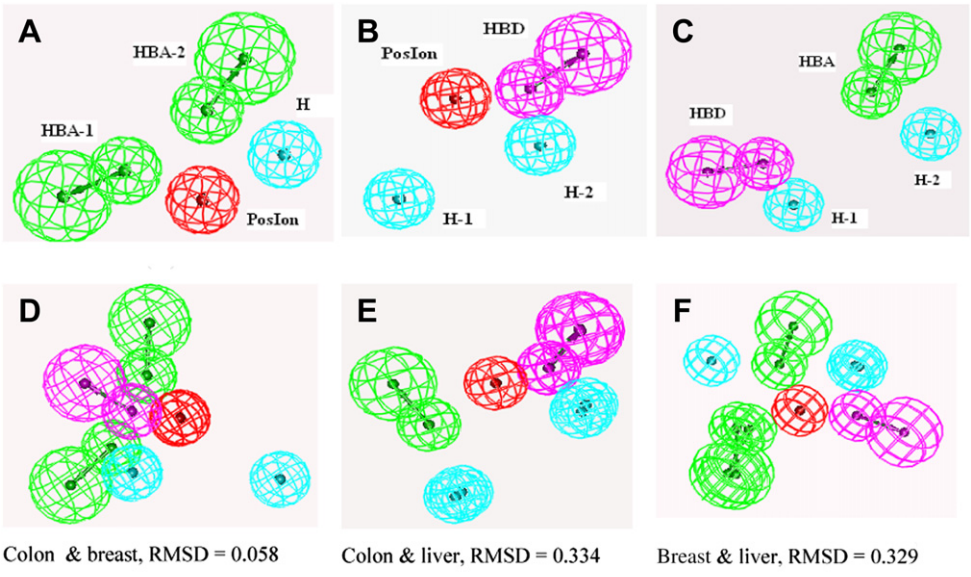


**Fig. 4.** (A–C), the generated 3D-pharmacophore model due to HCT116 (colon), MCF7 (breast) and HEPG2 (liver) cancer cell lines, respectively; (D–F) comparison between the generated pharmacophore models of the tested cancer cell lines.

QSAR analysis was employed to search for the best combination of orthogonal pharmacophores using a fit value and other structural descriptors (connectivity, topological, etc.) capable of explaining bioactivity variation across a collected list of the descriptors, allowing different pharmacophoric models competing within the 3D-QSAR framework.

A set of 13 compounds (**4a**–**f**,**h**–**k**,**m**–**o**) was used as a training set for a QSAR modeling. The remaining 2 compounds (**4g** and **4l**) were adopted as an external test subset for validating the QSAR models. Many molecular descriptors were calculated for each compound employing a calculate molecular properties module. The calculated descriptors including various simple and valence connectivity indices, electro-topological state indices, single point quantum-mechanical descriptors (via the AM1 model) and other molecular descriptors, were considered. Furthermore, the training set compounds were fitted against the corresponding pharmacophore hypotheses generated by the HYPOGEN automatic runs and their fit values (produced by the best-fit command) were added as additional molecular descriptors. Genetic function approximation (GFA) was employed to search for the best possible QSAR regression equation capable of correlating the variations in biological activities of the training set compounds with variations in the generated descriptors, i.e. multiple linear regression modeling (MLR) [30,35]. Equations (1)–(3) show our best-performing QSAR models (Figs. 5–7 exhibit the corresponding scatter plots of experimental versus estimated bioactivity values for the training set compounds against HCT116, MCF7 and HEPG2 tumor cell lines, respectively). The goodness of the model was validated by squared correlation coefficient ($R^2$) and residuals between the predicted and experimental activity of the test set and training set (Tables 6–8). $R^2$ values for HCT116 (colon), MCF7 (breast) and HEPG2 (liver) cancer QSAR models are 0.906, 0.856 and 0.923, respectively.

**Table 2**
Constraint distances (Å) and angles (°) between features of the generated pharmacophores.

| Cancer cell line | Constraint distances (Å) | Constraint angles (°) |
|---|---|---|
| HCT116 (colon) | (PosIon)-(HBA-1), 3.66; (PosIon)-(H), 4.76; (PosIon)-(HBA-2), 4.25; (HBA-1)-(HBA-2), 4.58; (HBA-2)-(H), 4.37 | (H)-(PosIon)-(HBA-1), 25.94; (PosIon)-(HBA-2)-(H), 109.01; (PosIon)-(HBA-1)-(HBA-2), 48.79 |
| MCF7 (breast) | (PosIon)-(HBD), 3.58; (PosIon)-(H-1), 6.46; (PosIon)-(H-2), 4.60; (HBD)-(H-2), 3.36; (H-1)-(H-2), 7.64 | (H-2)-(HBD)-(PosIon), 49.75; (H-2)-(PosIon)-(H-1), 36.92; (H-2)-(HBD)-( H-2), 22.25 |
| HEPG2 (liver) | (HBD)-(H-1), 3.08; (HBD)-(HBA), 7.20; (HBD)-(H-2), 9.19; (HBA)-(H-2), 4.17; (HBA)-(H-1), 8.05 | (H-1)-(HBD)-(HBA), 94.48; (H-2)-(HBA)-(HBD), 66.51; (H-1)-(HBD)-(H-2), 19.59 |

Equation (1)
Potency ($IC_{50}$) against HCT116 (colon cancer) cell line (N "number of molecules in the training set" = 13, $R^2$"squared correlation coefficient value" = 0.906)

$IC_{50}$ = 1320.335–160.262 [fit value] - 14.284 [LUMO-Eigen value-VAMP]

Equation (2)
Potency ($IC_{50}$) against MCF7 (breast cancer) cell line ($N$ = 13, $R^2$ = 0.856)

$IC_{50}$ = 1504.55 + 37.71 [shadow-nu] - 192.14 [fit value]

Equation (3)
Potency ($IC_{50}$) against HEPG2 (liver cancer) cell line ($N$ = 13, $R^2$ = 0.923)

$IC_{50}$ = 882.47–13.38 [pKa] - 106.68[fit value]

**Table 3**
Best fit values and estimated activities for compounds of the training set (**4a–f,h–k,m–o**) mapped with the generated 3D-pharmacophore model due to HCT-116 (colon) cancer cell line.

| Entry | Compd. | Estimated activity | Observed activity | Relative energy | Fit value |
|---|---|---|---|---|---|
| 1 | **4a** | 64.78 | 63.73 | 0.000 | 7.804 |
| 2 | **4b** | 40.62 | 33.05 | 1.203 | 8.007 |
| 3 | **4c** | 42.17 | 34.08 | 0.397 | 7.990 |
| 4 | **4d** | 43.79 | 36.80 | 4.733 | 7.974 |
| 5 | **4e** | 37.25 | 35.46 | 3.732 | 8.044 |
| 6 | **4f** | 35.31 | 47.40 | 19.095 | 8.067 |
| 7 | **4h** | 60.08 | 73.26 | 16.268 | 7.837 |
| 8 | **4i** | 34.97 | 31.31 | 7.402 | 8.072 |
| 9 | **4j** | 64.87 | 46.13 | 0.045 | 7.803 |
| 10 | **4k** | 83.08 | >126.31 | 0.032 | 7.696 |
| 11 | **4m** | 42.29 | 53.63 | 8.105 | 7.989 |
| 12 | **4n** | 53.86 | 41.03 | 6.441 | 7.884 |
| 13 | **4o** | 35.75 | 40.92 | 5.232 | 8.062 |

Searching for set descriptors (D), containing D descriptors of optimal subset (d), where d << D ones with minimum standard deviation (S), by means of multivariable linear regression technique:

$$\mathbf{S} = \frac{\mathbf{1}}{(\mathbf{N}-\mathbf{d}-\mathbf{1})}\sum_{\mathbf{i}=\mathbf{1}}^{\mathbf{N}}\mathbf{resi} \quad (1)$$

Where; N, is the number of molecules of the training set; resi, is the residual for molecule; i, is the difference between the experimental property (p) and predicted property (ppred).

More precisely, the Kubinyi function (FIT) [36,37] is a statistical parameter which is closely related to the Fisher ratio (F), but avoids the main disadvantage of the latter of being too sensitive to changes in small d values, and poorly sensitive to changes in large d values. The FIT (d) criterion has a low sensitivity to changes in small d values and a substantially increasing sensitivity for large d values. The greater the FIT value the better the linear equation [38]. It is given by the following equation, "where R (d) is the correlation coefficient for a model with (d) descriptors". The observed FIT values are 3.24, 2.95 and 3.45 corresponding to models due to HCT116, MCF7 and HEPG2 cancer cell lines, respectively (Table 9).

$$\mathbf{FIT} = \frac{\mathbf{R(d)^2(N-d-1)}}{\mathbf{(N+d^2)(1-R^2)}} \quad (2)$$

**Table 4**
Best fit values and estimated activities for compounds of the training set (**4a–f,h–k,m–o**) mapped with the generated 3D-pharmacophore model due to MCF-7 (breast) cancer cell line.

| Entry | Compd. | Estimated activity | Observed activity | Relative energy | Fit value |
|---|---|---|---|---|---|
| 1 | **4a** | 40.82 | 35.64 | 0.000 | 7.997 |
| 2 | **4b** | 43.25 | 38.66 | 0.252 | 7.972 |
| 3 | **4c** | 44.51 | 44.78 | 0.617 | 7.959 |
| 4 | **4d** | 38.43 | 43.03 | 0.000 | 8.023 |
| 5 | **4e** | 44.64 | 40.60 | 0.091 | 7.958 |
| 6 | **4f** | 40.07 | 38.73 | 0.848 | 8.005 |
| 7 | **4h** | 66.43 | 89.92 | 0.040 | 7.785 |
| 8 | **4i** | 52.69 | 43.96 | 0.319 | 7.886 |
| 9 | **4j** | 38.34 | 37.55 | 0.000 | 8.024 |
| 10 | **4k** | 40.93 | 49.92 | 0.226 | 7.996 |
| 11 | **4m** | 38.49 | 47.96 | 0.000 | 8.022 |
| 12 | **4n** | 45.16 | 38.14 | 0.108 | 7.953 |
| 13 | **4o** | 43.07 | 42.66 | 3.914 | 7.974 |

**Table 5**
Best fit values and estimated activities for compounds of the training set (**4a–f,h–k,m–o**) mapped with the generated 3D-pharmacophore model due to HEPG2 (liver) cancer cell line.

| Entry | Compd. | Estimated activity | Observed activity | Relative energy | Fit value |
|---|---|---|---|---|---|
| 1 | **4a** | 38.15 | 32.90 | 6.638 | 7.597 |
| 2 | **4b** | 33.90 | 33.05 | 1.264 | 7.648 |
| 3 | **4c** | 35.49 | 44.17 | 1.204 | 7.628 |
| 4 | **4d** | 51.74 | 32.42 | 6.612 | 7.465 |
| 5 | **4e** | 35.13 | 29.16 | 0.796 | 7.633 |
| 6 | **4f** | 33.36 | 43.37 | 14.250 | 7.655 |
| 7 | **4h** | 45.58 | 41.09 | 0.040 | 7.520 |
| 8 | **4i** | 31.94 | 27.69 | 0.654 | 7.674 |
| 9 | **4j** | 94.47 | 77.09 | 0.000 | 7.203 |
| 10 | **4k** | 58.96 | 63.16 | 4.649 | 7.408 |
| 11 | **4m** | 57.09 | 72.55 | 8.621 | 7.422 |
| 12 | **4n** | 25.71 | 28.89 | 14.558 | 7.768 |
| 13 | **4o** | 37.34 | 49.68 | 2.704 | 7.606 |

*2.3.3. Validation of QSAR*

External validation of the determined QSAR equations was performed utilizing two of our synthesized analogues exhibiting mild (**4g**) and promising (**4l**) anti-tumor properties. The observed activities and those provides by QSAR study, are presented in Table 10.

## 3. Conclusion

1,3-Dipolar cycloaddition reaction of 1-aryl-1*H*-pyrrole-2,5-diones **1a–e** with non-stabilized azomethine ylides, generated in situ via decarboxylative condensation of isatins **2a–c** and sarcosine (**3**) as a representative example of α-amino acid afforded 4′-aryl-5′*a*,6′-dihydro-1′-methyl-spiro[3*H*-indole-3,2′(1′*H*)-pyrrolo[3,4-*c*]pyrrole]-2,3′,5′(1*H*,2′*aH*,4′*H*)-triones **4a–o** in good yields (71–90%). Most of the synthesized compounds revealed moderate anti-tumor properties against HCT116 (colon), MCF7 (breast) and HEPG2 (liver) human tumor cell lines, while compound **4l** exhibited considerable anti-tumor activity against HEPG2 (liver cancer) cell line ($IC_{50}$ = 12.16 μM), comparable to that of Doxorubicin ($IC_{50}$ = 7.36 μM). 3D-QSAR pharmacophore modeling utilizing 13 compounds (**4a–f,h–k,m–o**) as a training set afforded an HYPOGEN of four chemical features: two hydrogen bond acceptors, one hydrophobic and one positive ionizable, in case of HCT116 (colon) cancer cell line. For MCF7 (breast) cancer cell line two hydrophobics, one positive ionisable, and one hydrogen bond donor features were observed and for HEPG2 (liver) cancer cell line two hydrophobics, one hydrogen bond donor and one hydrogen bond acceptor features, were recognized.

Classical QSAR studies delivered equations of two descriptors with $R^2$ = 0.906, 0.856, 0.923, in case of HCT116 (colon), MCF7 (breast) and HEPG2 (liver) cancer cell lines, respectively. The most important descriptor in all the equations was the fit value derived from mapping of the synthesized analogue into the generated pharmacophore. The other controlling descriptors were LUMO-Eigen value-VAMP (in case of HCT116 cell line), shadow-nu (in case of MCF7 cell line) and pKa (in case of HEPG2 cell line).

External validation of the established QSAR models utilizing two of our synthesized analogues exhibiting mild (**4g**) and promising (**4l**) anti-tumor properties, revealed good agreement between the experimental and the calculated data. It can be concluded that combination of 3D-pharmacophore modeling and QSAR provides as an effective technique for understanding the observed pharmacological properties and thus could be adopted for developing effective lead structures.

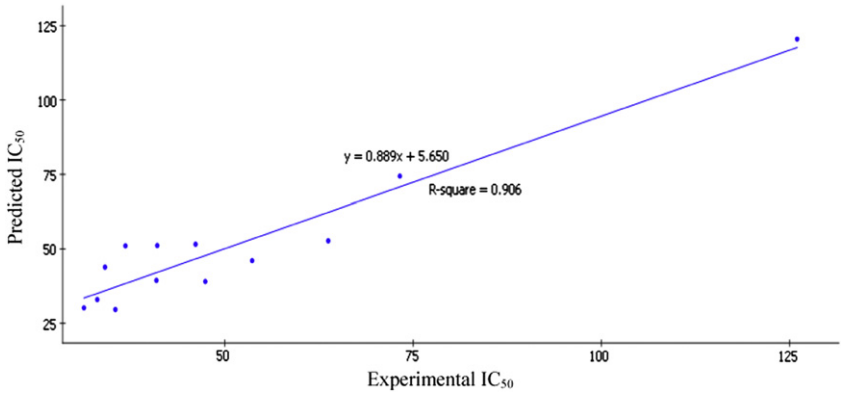


**Fig. 5.** Predicted versus experimental $IC_{50}$ of the tested compounds against HCT116 (colon) human tumor cell line.

## 4. Experimental protocols

Melting points were recorded on a Stuart SMP3 melting point apparatus. IR spectra (KBr) were recorded on JASCO 6100 and Shimadzu 8400S FT-IR spectrophotometers. $^1$H NMR, as well as 2D-NMR spectra were recorded on a Varian MERCURY VX300 ($^1$H: 300,$^{13}$C: 75 MHz) spectrometer in DMSO-$d_6$. $^{13}$C NMR spectra were recorded on Varian MERCURY 300BB (75 MHz) and JEOL AS 500 (125 MHz) spectrometers in DMSO-$d_6$. Mass spectra were recorded on a Shimadzu GCMS-QP 1000 EX (EI, 70 eV) spectrometer. The starting compounds **1a**–**e** [39–41] were prepared according to the previously reported procedures.

### *4.1. Synthesis of 4′-aryl-5′a,6′-dihydro-1′-methyl-spiro[3H-indole-3,2′(1′H)-pyrrolo[3,4-c]pyrrole]-2,3′,5′(1H,2′aH,4′H)-triones **4a**–**o** (general procedure)*

A mixture of equimolar amounts of the appropriate **1a**–**e** (5 mmol), the corresponding **2a**–**c** and sarcosine (**3**) in absolute ethanol (25 ml) was boiled under reflux for the appropriate time. The separated solid while refluxing was collected and crystallized from a suitable solvent affording the corresponding **4b**–**i,k**–**o**. In case of **4a,j** the clear reaction mixture was stored at room temperature (20–25 °C) overnight and the separated solid was collected and crystallized from a suitable solvent.

#### *4.1.1. 5′a,6′-Dihydro-1′-methyl-4′-phenyl-spiro[3H-indole-3,2′(1′H)-pyrrolo[3,4-c]pyrrole]-2,3′,5′(1H,2′aH,4′H)-trione (**4a**)*

Reaction time 6 h, colorless crystals from n-butanol, mp 259–261 °C, yield (1.3 g) 75%. IR: $\nu_{max}$/cm$^{-1}$ 3166 (NH), 1709 (br, C=O), 1618, 1496. $^1$H NMR: $\delta$ 2.00 (s, 3H, $NCH_3$), 3.36 (d, 1H, upfield H of $CH_2$, $J$ = 9.9 Hz), 3.55 (d, 1H, *H*-2′*a*, $J$ = 8.4 Hz), 3.63 (pseudo t, 1H, downfield H of $CH_2$, $J$ = 8.25 Hz), 3.75 (pseudo t, 1H, *H*-5′*a*, $J$ = 7.95 Hz), 6.84–7.56 (m, 9H, arom. H), 10.57 (s, 1H, NH). $^{13}$C NMR: $\delta$ 34.3 ($NCH_3$), 44.6 (*HC*-5′*a*), 52.0 (*HC*-2′*a*), 54.1 ($H_2C$-6′), 72.2 [spiro *C*-3 (*C*-2′)], 109.7, 121.7, 125.2, 125.9, 126.8, 128.4, 129.0, 129.6, 132.3, 142.7 (arom. *C*), 174.0, 177.8, 178.1 (C=O). MS: *m/z* (%) 347 (M, 100), 318 (87), 317 (23), 227 (18), 199 (62), 198 (28), 172 (76), 171 (70). Anal. Calcd. for $C_{20}H_{17}N_3O_3$ (347.38): C, 69.15; H, 4.93; N, 12.10. Found: C, 69.36; H, 5.04; N, 12.18.

#### *4.1.2. 5-Chloro-5′a,6′-dihydro-1′-methyl-4′-phenyl-spiro[3H-indole-3,2′(1′H)-pyrrolo[3,4-c]pyrrole]-2,3′,5′(1H,2′aH,4′H)-trione (**4b**)*

Reaction time 5 h, colorless crystals from n-butanol, mp 262–264 °C, yield (1.7 g) 89%. IR: $\nu_{max}$/cm$^{-1}$ 3283 (NH), 1705 (br, C=O), 1620, 1477. $^1$H NMR: $\delta$ 2.03 (s, 3H, $NCH_3$), 3.38 (d, 1H, upfield H of $CH_2$, $J$ = 9.0 Hz), 3.60 (d, 1H, *H*-2′*a*, $J$ = 8.1 Hz), 3.77 (pseudo t, 1H, downfield H of $CH_2$, $J$ = 7.95 Hz), 3.90 (br s, 1H, *H*-5′*a*), 6.85–7.57 (m, 8H, arom. H), 10.73 (s, 1H, NH). MS: *m/z* (%) 381 (M, 100), 383 [(M+2), 36], 352 (67), 351 (7), 261 (15), 233 (54), 232 (17), 206 (70), 205 (43). Anal. Calcd. for $C_{20}H_{16}ClN_3O_3$ (381.82): C, 62.91; H, 4.22; N, 11.01. Found: C, 62.98; H, 4.31; N, 11.13.

#### *4.1.3. 5′a,6′-Dihydro-5-methoxy-1′-methyl-4′-phenyl-spiro[3H-indole-3,2′(1′H)-pyrrolo[3,4-c]pyrrole]-2,3′,5′(1H,2′aH,4′H)-trione (**4c**)*

Reaction time 9 h, colorless crystals from n-butanol, mp 216–218 °C, yield (1.5 g) 80%. IR: $\nu_{max}$/cm$^{-1}$ 3159 (NH), 1708 (br, C=O), 1604, 1495. $^1$H NMR: $\delta$ 2.01 (s, 3H, $NCH_3$), 3.37 (d, 1H, upfield H of

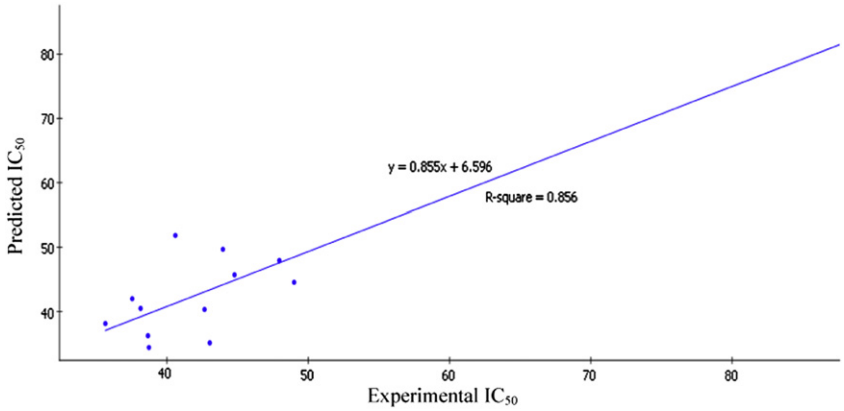


**Fig. 6.** Predicted versus experimental $IC_{50}$ of the tested compounds against MCF7 (breast) human tumor cell line.

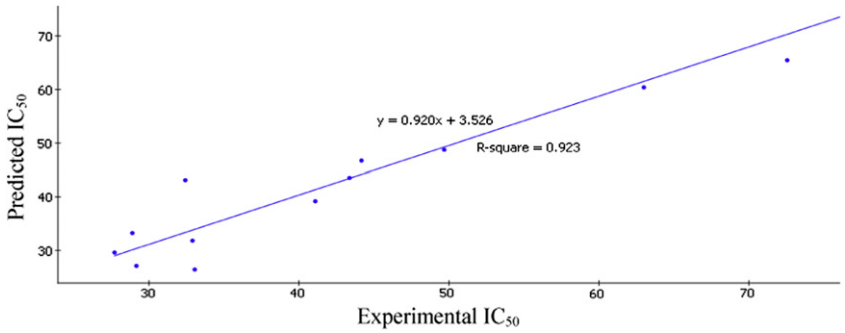


**Fig. 7.** Predicted versus experimental $IC_{50}$ of the tested compounds against HEPG2 (liver) human tumor cell line.

$CH_2$, $J$ = 7.8 Hz), 3.55 (d, 1H, *H*-2′*a*, $J$ = 8.4 Hz), 3.60 (s, 3H, $OCH_3$), 3.75 (br s, 1H, downfield H of $CH_2$), 3.85 (pseudo t, 1H, *H*-5′*a*, $J$ = 9.6 Hz), 6.75–7.56 (m, 8H, arom. H), 10.37 (s, 1H, NH). MS: *m/z* (%) 377 (M, 38), 257 (21), 229 (31), 228 (21), 202 (19). Anal. Calcd. for $C_{21}H_{19}N_3O_4$ (377.40): C, 66.83; H, 5.07; N, 11.13. Found: C, 66.67; H, 5.03; N, 11.29.

#### 4.1.4. 4′-(4-Chlorophenyl)-5′a,6′-dihydro-1′-methyl-spiro[3H-indole-3,2′(1′H)-pyrrolo[3,4-c]pyrrole]-2,3′,5′(1H,2′aH,4′H)-trione (**4d**)

Reaction time 12 h, colorless crystals from n-butanol, mp 272–274 °C, yield (1.4 g) 73%. IR: $\nu_{max}/cm^{-1}$ 3173 (NH), 1712 (br, C=O), 1617, 1481. $^1$H NMR: $\delta$ 1.99 (s, 3H, $NCH_3$), 3.35 (d, 1H, upfield H of $CH_2$, $J$ = 9.3 Hz), 3.54 (d, 1H, *H*-2′*a*, $J$ = 8.4 Hz), 3.63 (pseudo t, 1H, downfield H of $CH_2$, $J$ = 8.4 Hz), 3.75 (pseudo t, 1H, *H*-5′*a*, $J$ = 7.8 Hz), 6.83–7.61 (m, 8H, arom. H), 10.57 (s, 1H, NH). $^{13}$C NMR: $\delta$ 34.9 ($NCH_3$), 45.2 (*HC*-5′*a*), 52.5 (*HC*-2′*a*), 54.6 ($H_2C$-6′), 72.7 [spiro *C*-3 (*C*-2′)], 110.3, 122.2, 125.6, 126.5, 129.1, 129.7, 130.2, 131.6, 133.5, 143.3 (arom. *C*), 174.4, 178.3, 178.5 (*C*=O). MS: *m/z* (%) 381 (M, 89), 383 [(M+2), 27], 352 (81), 351 (2), 227 (23), 199 (87), 198 (24), 172 (100), 171 (92). Anal. Calcd. for $C_{20}H_{16}ClN_3O_3$ (381.82): C, 62.91; H, 4.22; N, 11.01. Found: C, 63.11; H, 4.38; N, 11.10.

#### 4.1.5. 5-Chloro-4′-(4-chlorophenyl)-5′a,6′-dihydro-1′-methyl-spiro[3H-indole-3,2′(1′H)-pyrrolo[3,4-c]pyrrole]-2,3′,5′(1H,2′aH,4′H)-trione (**4e**)

Reaction time 7 h, colorless crystals from n-butanol, mp 280–282 °C, yield (1.8 g) 87%. IR: $\nu_{max}/cm^{-1}$ 3157 (NH), 1712 (br, C=O), 1616, 1488. $^1$H NMR: $\delta$ 2.00 (s, 3H, $NCH_3$), 3.35 (d, 1H, upfield H of $CH_2$, $J$ = 7.8 Hz), 3.59 (d, 1H, *H*-2′*a*, $J$ = 8.4 Hz), 3.87 (br s, 2H, downfield H of $CH_2$ + *H*-5′*a*), 6.83–7.64 (m, 7H, arom. H), 10.71 (s, 1H, NH). MS: *m/z* (%) 415 (M, 100), 419 [(M+4), 11], 417 [(M+2), 60], 386 (76), 385 (66), 261 (26), 233 (87), 232 (66), 206 (97), 205 (60). Anal. Calcd. for $C_{20}H_{15}Cl_2N_3O_3$ (416.27): C, 57.71; H, 3.63; N, 10.09. Found: C, 57.65; H, 3.53; N, 9.95.

#### 4.1.6. 4′-(4-Chlorophenyl)-5′a,6′-dihydro-5-methoxy-1′-methyl-spiro[3H-indole-3,2′(1′H)-pyrrolo[3,4-c]pyrrole]-2,3′,5′(1H,2′aH,4′H)-trione (**4f**)

Reaction time 9 h, colorless crystals from n-butanol, mp 245–247 °C, yield (1.6 g) 78%. IR: $\nu_{max}/cm^{-1}$ 3150 (NH), 1711 (br, C=O), 1610, 1493. $^1$H NMR: $\delta$ 2.00 (s, 3H, $NCH_3$), 3.36 (d, 1H, upfield H of $CH_2$, $J$ = 8.4 Hz), 3.48 (d, 1H, *H*-2′*a*, $J$ = 8.7 Hz), 3.53 (pseudo t, 1H, downfield H of $CH_2$, $J$ = 9.15 Hz), 3.75 (s, 3H, $OCH_3$), 3.85 (pseudo t, 1H, *H*-5′*a*, $J$ = 9.0 Hz), 6.75–7.59 (m, 7H, arom. H), 10.37 (s, 1H, NH). MS: *m/z* (%) 411 (M, 71), 413 [(M+2), 23], 382 (29), 381 (3), 257 (25), 229 (71), 228 (16), 202 (60), 201 (26). Anal. Calcd. for $C_{21}H_{18}ClN_3O_4$ (411.85): C, 61.24; H, 4.41; N, 10.20. Found: C, 61.40; H, 4.51; N, 10.01.

#### 4.1.7. 5′a,6′-Dihydro-4′-(4-fluorophenyl)-1′-methyl-spiro[3H-indole-3,2′(1′H)-pyrrolo[3,4-c]pyrrole]-2,3′,5′(1H,2′aH,4′H)-trione (**4g**)

Reaction time 10 h, colorless crystals from n-butanol, mp 234–236 °C, yield (1.3 g) 71%. IR: $\nu_{max}/cm^{-1}$ 3176 (NH), 1709 (br, C=O), 1615, 1510. $^1$H NMR: $\delta$ 1.99 (s, 3H, $NCH_3$), 3.33 (d, 1H, upfield H of $CH_2$, $J$ = 8.4 Hz), 3.45 (d, 1H, *H*-2′*a*, $J$ = 8.4 Hz), 3.56 (pseudo t, 1H, downfield H of $CH_2$, $J$ = 8.85 Hz), 3.73 (pseudo t, 1H, *H*-5′*a*, $J$ = 7.8 Hz), 6.83–7.38 (m, 8H, arom. H), 10.55 (s, 1H, NH). MS: *m/z* (%) 365 (M, 100), 336 (80), 335 (13), 227 (16), 199 (63), 198 (43), 172 (81), 171 (74). Anal. Calcd. for $C_{20}H_{16}FN_3O_3$ (365.37): C, 65.75; H, 4.41; N, 11.50. Found: C, 65.64; H, 4.28; N, 11.43.

**Table 6**
Estimated activity data of the training set against HCT116 (colon cancer) cell line and calculated descriptors governing activity according to Equation (1).

| Entry | Compd. | Estimated activity | Observed activity | Residuals | LUMO | Fit value |
|---|---|---|---|---|---|---|
| 1 | **4a** | 71.48 | 63.73 | −7.752 | −0.127 | 7.804 |
| 2 | **4b** | 41.94 | 33.05 | −8.887 | −0.332 | 8.007 |
| 3 | **4c** | 40.95 | 34.08 | −6.872 | −0.081 | 7.990 |
| 4 | **4d** | 44.87 | 36.80 | −8.068 | −0.172 | 7.974 |
| 5 | **4e** | 37.84 | 35.46 | −2.379 | −0.468 | 8.044 |
| 6 | **4f** | 29.58 | 47.40 | 17.824 | −0.150 | 8.067 |
| 7 | **4h** | 69.44 | 73.26 | 3.823 | −0.350 | 7.837 |
| 8 | **4i** | 30.48 | 31.31 | 0.835 | −0.260 | 8.072 |
| 9 | **4j** | 71.38 | 46.13 | −25.250 | −0.113 | 7.803 |
| 10 | **4k** | 92.18 | >126.31 | 33.822 | −0.363 | 7.696 |
| 11 | **4m** | 40.79 | 53.63 | 12.845 | −0.056 | 7.989 |
| 12 | **4n** | 62.41 | 41.03 | −21.379 | −0.391 | 7.884 |
| 13 | **4o** | 29.48 | 40.92 | 11.438 | −0.082 | 8.062 |

**Table 7**
Estimated activity data of the training set against MCF7 (breast cancer) cell line and calculated descriptors governing activity according to Equation (2).

| Entry | Compd. | Estimated activity | Observed activity | Residuals | Shadow -nu | Fit value |
|---|---|---|---|---|---|---|
| 1 | **4a** | 38.42 | 35.64 | −2.784 | 1.820 | 7.997 |
| 2 | **4b** | 36.56 | 38.66 | 2.096 | 1.691 | 7.972 |
| 3 | **4c** | 45.09 | 44.78 | −0.308 | 1.804 | 7.959 |
| 4 | **4d** | 34.45 | 43.03 | 8.577 | 1.990 | 8.023 |
| 5 | **4e** | 51.66 | 40.60 | −11.057 | 1.922 | 7.958 |
| 6 | **4f** | 35.26 | 38.73 | 3.474 | 1.866 | 8.005 |
| 7 | **4h** | 84.41 | 89.92 | 5.507 | 1.830 | 7.785 |
| 8 | **4i** | 49.47 | 43.96 | −5.507 | 1.787 | 7.886 |
| 9 | **4j** | 42.37 | 37.55 | −4.818 | 1.979 | 8.024 |
| 10 | **4k** | 44.18 | 49.92 | 4.818 | 1.908 | 7.996 |
| 11 | **4m** | 47.94 | 47.96 | 0.023 | 2.064 | 8.022 |
| 12 | **4n** | 40.50 | 38.14 | −2.359 | 1.990 | 7.953 |
| 13 | **4o** | 40.32 | 42.66 | 2.339 | 1.978 | 7.974 |

**Table 8**
Estimated activity data of the training set against HEPG2 (liver cancer) cell line and calculated descriptors governing activity according to Equation (3).

| Entry | Compd. | Estimated activity | Observed activity | Residuals | PKa | Fit value |
|---|---|---|---|---|---|---|
| 1 | **4a** | 31.82 | 32.90 | 1.080 | 1.90 | 7.597 |
| 2 | **4b** | 26.44 | 33.05 | 6.612 | 2.23 | 7.648 |
| 3 | **4c** | 46.71 | 44.17 | −2.540 | 2.23 | 7.628 |
| 4 | **4d** | 43.12 | 32.42 | −10.701 | 1.90 | 7.465 |
| 5 | **4e** | 27.12 | 29.16 | 2.043 | 1.90 | 7.633 |
| 6 | **4f** | 43.53 | 43.37 | −0.160 | 2.23 | 7.655 |
| 7 | **4h** | 39.18 | 41.09 | 1.911 | 1.93 | 7.520 |
| 8 | **4i** | 29.60 | 27.69 | −1.911 | 1.90 | 7.674 |
| 9 | **4j** | 79.71 | 77.09 | −2.618 | 1.90 | 7.203 |
| 10 | **4k** | 60.38 | 63.16 | 2.617 | 2.62 | 7.408 |
| 11 | **4m** | 65.46 | 72.55 | 7.086 | 1.93 | 7.422 |
| 12 | **4n** | 33.26 | 28.89 | −4.365 | 1.90 | 7.768 |
| 13 | **4o** | 48.74 | 49.68 | 0.945 | 2.62 | 7.606 |

#### *4.1.8. 5-Chloro-5′a,6′-dihydro-4′-(4-fluorophenyl)-1′-methyl-spiro[3H-indole-3,2′(1′H)-pyrrolo[3,4-c]pyrrole]-2,3′,5′(1H,2′aH,4′H)-trione (**4h**)*

Reaction time 8 h, colorless crystals from n-butanol, mp 294–296 °C, yield (1.8 g) 90%. IR: $\nu_{max}/cm^{-1}$ 3114 (NH), 1709 (br, C=O), 1621, 1509. $^1$H NMR: $\delta$ 2.03 (s, 3H, $NCH_3$), 3.37 (d, 1H, upfield H of $CH_2$, $J$ = 8.4 Hz), 3.59 (d, 1H, *H*-2′*a*, $J$ = 8.4 Hz), 3.75 (pseudo t, 1H, downfield H of $CH_2$, $J$ = 7.95 Hz), 3.89 (br s, 1H, *H*-5′*a*), 6.84–7.48 (m, 7H, arom. H), 10.73 (s, 1H, NH). MS: *m/z* (%) 399 (M, 100), 401 [(M+2), 33], 370 (60), 369 (40), 261 (17), 233 (65), 232 (19), 206 (70), 205 (37). Anal. Calcd. for $C_{20}H_{15}ClFN_3O_3$ (399.81): C, 60.08; H, 3.78; N, 10.51. Found: C, 59.99; H, 3.72; N, 10.38.

#### *4.1.9. 5′a,6′-Dihydro-4′-(4-fluorophenyl)-5-methoxy-1′-methyl-spiro[3H-indole-3,2′(1′H)-pyrrolo[3,4-c]pyrrole]-2,3′,5′(1H,2′aH,4′H)-trione (**4i**)*

Reaction time 10 h, colorless crystals from n-butanol, mp 244–246 °C, yield (1.7 g) 86%. IR: $\nu_{max}/cm^{-1}$ 3158 (NH), 1706 (br, C=O), 1610, 1501. $^1$H NMR: $\delta$ 2.02 (s, 3H, $NCH_3$), 3.36 (d, 1H, upfield H of $CH_2$, $J$ = 8.7 Hz), 3.54 (d, 1H, *H*-2′*a*, $J$ = 8.1 Hz), 3.60 (s, 3H, $OCH_3$), 3.75 (br s, 2H, downfield H of $CH_2$+ *H*-5′*a*), 6.42–7.38 (m, 7H, arom. H), 10.40 (s, 1H, NH). MS: *m/z* (%) 395 (M, 65), 366 (29), 365 (8), 257 (16), 229 (52), 228 (10), 202 (47), 201 (18). Anal. Calcd. for $C_{21}H_{18}FN_3O_4$ (395.39): C, 63.79; H, 4.59; N, 10.63. Found: C, 63.60; H, 4.51; N, 10.67.

#### *4.1.10. 5′a,6′-Dihydro-1′-methyl-4′-(4-methylphenyl)-spiro[3H-indole-3,2′(1′H)-pyrrolo[3,4-c]pyrrole]-2,3′,5′(1H,2′aH,4′H)-trione (**4j**)*

Reaction time 12 h, colorless crystals from n-butanol, mp 207–209 °C, yield (1.3 g) 72%. IR: $\nu_{max}/cm^{-1}$ 3174 (NH), 1712 (br, C=O), 1614, 1514. $^1$H NMR: $\delta$ 1.99 (s, 3H, $NCH_3$), 2.34 (s, 3H, $ArCH_3$), 3.35 (d, 1H, upfield H of $CH_2$, $J$ = 9.0 Hz), 3.53 (d, 1H, *H*-2′*a*, $J$ = 8.1 Hz), 3.62 (pseudo t, 1H, downfield H of $CH_2$, $J$ = 8.25 Hz), 3.73 (pseudo t, 1H, *H*-5′*a*, $J$ = 7.95 Hz), 6.83–7.34 (m, 8H, arom. H), 10.55 (s, 1H, NH). MS: *m/z* (%) 361 (M, 100), 332 (90), 227 (37), 199 (84), 198 (45), 172 (100), 171 (74). Anal. Calcd. for $C_{21}H_{19}N_3O_3$ (361.40): C, 69.79; H, 5.30; N, 11.63. Found: C, 69.72; H, 5.21; N, 11.47.

**Table 9**
Linear QSAR models established for the training set ($N$ = 13).

| Cell lines | Descriptors | R | S | FIT |
|---|---|---|---|---|
| HCT116 (colon) | Fit value, LUMO-Eigen value-VAMP | 0.9541 | 0.675 | 3.24 |
| MCF7 (breast) | Fit value, Shadow-nu | 0.925 | 0.764 | 2.95 |
| HEPG2 (liver) | Fit value, PKa | 0.960 | 0.498 | 3.45 |

#### *4.1.11. 5-Chloro-5′a,6′-dihydro-1′-methyl-4′-(4-methylphenyl)-spiro[3H-indole-3,2′(1′H)-pyrrolo[3,4-c]pyrrole]-2,3′,5′(1H,2′aH,4′H)-trione (**4k**)*

Reaction time 8 h, colorless crystals from n-butanol, mp 266–268 °C, yield (1.6 g) 81%. IR: $\nu_{max}/cm^{-1}$ 3275 (NH), 1707 (br, C=O), 1617, 1511. $^1$H NMR: $\delta$ 2.03 (s, 3H, $NCH_3$), 2.36 (s, 3H, $ArCH_3$), 3.37 (d, 1H, upfield H of $CH_2$, $J$ = 9.0 Hz), 3.58 (d, 1H, *H*-2′*a*, $J$ = 8.4 Hz), 3.74 (pseudo t, 1H, downfield H of $CH_2$, $J$ = 7.8 Hz), 3.87 (br s, 1H, *H*-5′*a*), 6.82–7.47 (m, 7H, arom. H), 10.72 (s, 1H, NH). MS: *m/z* (%) 395 (M, 64), 397 [(M+2), 42], 366 (52), 365 (48), 261 (10), 233 (46), 232 (22), 206 (56), 205 (32). Anal. Calcd. for $C_{21}H_{18}ClN_3O_3$ (395.85): C, 63.72; H, 4.58; N, 10.62. Found: C, 63.86; H, 4.61; N, 10.60.

#### *4.1.12. 5′a,6′-Dihydro-5-methoxy-1′-methyl-4′-(4-methylphenyl)-spiro[3H-indole-3,2′(1′H)-pyrrolo[3,4-c]pyrrole]-2,3′,5′(1H,2′aH,4′H)-trione (**4l**)*

Reaction time 10 h, colorless crystals from n-butanol, mp 247–249 °C, yield (1.5 g) 77%. IR: $\nu_{max}/cm^{-1}$ 3156 (NH), 1714 (br, C=O), 1610, 1490. $^1$H NMR: $\delta$ 2.01 (s, 3H, $NCH_3$), 2.36 (s, 3H, $ArCH_3$), 3.35 (d, 1H, upfield H of $CH_2$, $J$ = 9.3 Hz), 3.51 (pseudo t, 1H, *H*-2′*a*, $J$ = 8.4 Hz), 3.61 (s, 3H, $OCH_3$), 3.75 (br s, 2H, downfield H of $CH_2$ + *H*-5′*a*), 6.42–7.34 (m, 7H, arom. H), 10.39 (s, 1H, NH). MS: *m/z* (%) 391 (M, 98), 362 (42), 361 (23), 257 (28), 229 (95), 228 (39), 202 (72), 201 (34). Anal. Calcd. for $C_{22}H_{21}N_3O_4$ (391.43): C, 67.51; H, 5.41; N, 10.74. Found: C, 67.28; H, 5.30; N, 10.67.

#### *4.1.13. 5′a,6′-Dihydro-4′-(4-methoxyphenyl)-1′-methyl-spiro[3H-indole-3,2′(1′H)-pyrrolo[3,4-c]pyrrole]-2,3′,5′(1H,2′aH,4′H)-trione (**4m**)*

Reaction time 8 h, colorless crystals from n-butanol, mp 276–278 °C, yield (1.4 g) 74%. IR: $\nu_{max}/cm^{-1}$ 3317 (NH), 1710 (br, C=O), 1608, 1511. $^1$H NMR: $\delta$ 1.99 (s, 3H, $NCH_3$), 3.34 (d, 1H, upfield H of $CH_2$, $J$ = 8.1 Hz), 3.52 (d, 1H, *H*-2′*a*, $J$ = 8.1 Hz), 3.61 (pseudo t, 1H, downfield H of $CH_2$, $J$ = 8.25 Hz), 3.72 (pseudo t, 1H, *H*-5′*a*, $J$ = 8.4 Hz), 3.80 (s, 3H, $OCH_3$), 6.83–7.25 (m, 8H, arom. H), 10.55 (s, 1H, NH). $^{13}$C NMR: $\delta$ 34.9 ($NCH_3$), 45.1 (*HC*-5′*a*), 52.4 (*HC*-2′*a*), 54.6 ($H_2C$-6′), 55.9 ($OCH_3$), 72.7 [spiro *C*-3 (*C*-2′)], 110.3, 114.8, 122.2, 125.4, 125.8, 126.5, 128.6, 130.1, 143.3, 159.5 (arom. *C*), 174.8, 178.4, 178.9 (*C*=O). MS: *m/z* (%) 377 (M, 78), 348 (50), 347 (4), 227 (9), 199 (100), 198 (9), 172 (74), 171 (61). Anal. Calcd. for $C_{21}H_{19}N_3O_4$ (377.40): C, 66.83; H, 5.07; N, 11.13. Found: C, 66.77; H, 4.99; N, 11.24.

#### *4.1.14. 5-Chloro-5′a,6′-dihydro-4′-(4-methoxyphenyl)-1′-methyl-spiro[3H-indole-3,2′(1′H)-pyrrolo[3,4-c]pyrrole]-2,3′,5′(1H,2′aH,4′H)-trione (**4n**)*

Reaction time 8 h, colorless crystals from n-butanol, mp 283–285 °C, yield (1.8 g) 88%. IR: $\nu_{max}/cm^{-1}$ 3300 (NH), 1708 (br, C=O), 1614, 1512. $^1$H NMR: $\delta$ 2.02 (s, 3H, $NCH_3$), 3.36 (d, 1H, upfield H of $CH_2$, $J$ = 9.0 Hz), 3.57 (d, 1H, *H*-2′*a*, $J$ = 8.1 Hz), 3.59 (pseudo t, 1H, downfield H of $CH_2$, $J$ = 9.0 Hz), 3.73 (pseudo t, 1H, *H*-5′*a*, $J$ = 8.1 Hz), 3.81 (s, 3H, $OCH_3$), 6.83–7.33 (m, 7H, arom. H), 10.72 (s, 1H, NH). $^{13}$C NMR: $\delta$ 35.0 ($NCH_3$), 45.0 (*HC*-5′*a*), 52.6 (*HC*-2′*a*), 54.8 ($H_2C$-6′), 56.0 ($OCH_3$), 72.7 [spiro *C*-3 (*C*-2′)], 111.8, 114.9, 125.3, 126.1, 126.3, 128.0, 128.5, 130.1, 142.2, 159.6 (arom. *C*), 174.8, 178.0, 178.7 (*C*=O). MS: *m/z* (%) 411 (M, 93), 413 [(M+2), 31], 382 (45), 381 (2), 261 (10), 233 (100), 232 (7), 206 (79), 205 (43). Anal. Calcd. for $C_{21}H_{18}ClN_3O_4$ (411.85): C, 61.24; H, 4.41; N, 10.20. Found: C, 61.36; H, 4.51; N, 10.14.

#### *4.1.15. 5′a,6′-Dihydro-5-methoxy-4′-(4-methoxyphenyl)-1′-methyl-spiro[3H-indole-3,2′(1′H)-pyrrolo[3,4-c]pyrrole]-2,3′,5′(1H,2′aH,4′H)-trione (**4o**)*

Reaction time 10 h, colorless crystals from n-butanol, mp 252–254 °C, yield (1.5 g) 74%. IR: $\nu_{max}/cm^{-1}$ 3276 (NH), 1711 (br, C=

**Table 10**
External validation for the established QSAR models utilizing mild (**4g**) and promising (**4l**) anti-tumor active agents.

| Cell lines | Compd. | 3D-QSAR pharmacophore | | | Classical QSAR | | | | |
|---|---|---|---|---|---|---|---|---|---|
| | | Experimental activity ($IC_{50}$) | Predicted activity ($IC_{50}$) | Fit value | Experimental activity ($IC_{50}$) | Predicted activity ($IC_{50}$) | LUMO | Shadow-nu | PKa |
| HCT116 (colon) | **4g** | 42.37 | 46.10 | 8.01 | 42.37 | 40.80 | −0.294 | – | – |
| | **4l** | 46.24 | 50.13 | 7.98 | 46.24 | 44.87 | −0.353 | – | – |
| MCF7 (breast) | **4g** | 33.88 | 37.45 | 8.02 | 33.88 | 33.18 | – | 1.842 | – |
| | **4l** | 46.83 | 41.96 | 7.95 | 46.83 | 48.25 | – | 1.889 | – |
| HEPG2 (liver) | **4g** | 87.31 | 90.32 | 7.22 | 87.31 | 86.42 | – | – | 1.93 |
| | **4l** | 12.16 | 10.26 | 7.91 | 12.16 | 13.22 | – | – | 1.90 |

O), 1607, 1509. $^1$H NMR: $\delta$ 2.01 (s, 3H, $NCH_3$), 3.35 (d, 1H, upfield H of $CH_2$, $J$ = 8.1 Hz), 3.52 (d, 1H, *H*-2′*a*, $J$ = 8.4 Hz), 3.61 (s, 3H, $OCH_3$), 3.75 (br s, 1H, downfield H of $CH_2$), 3.79 (br s, 1H, *H*-5′*a*), 3.80 (s, 3H, $OCH_3$), 6.42–7.22 (m, 7H, arom. H), 10.39 (s, 1H, NH). MS: *m/z* (%) 407 (M, 70), 378 (23), 377 (2), 257 (11), 229 (100), 228 (22), 202 (56), 201 (20). Anal. Calcd. for $C_{22}H_{21}N_3O_5$ (407.43): C, 64.86; H, 5.20; N, 10.31. Found: C, 64.76; H, 5.09; N, 10.23.

### 4.2. Single crystal X-ray crystallography

Full crystallographic details, excluding structure factors have been deposited at Cambridge Crystallographic Data Centre (CCDC) as supplementary publication numbers CCDC 846811 & 846812 corresponding to compounds **4a** and **4m**, respectively. The crystallographic data were collected at $T$ = 298 K on a Kappa CCD Enraf Nonius FR 590 diffractometer using a graphite monochromator with Mo-$K_\alpha$ radiation ($\lambda$ = 0.71073 Å). The crystal structures were determined by direct method using SIR92 [42] and refined by maXus [43] (Bruker Nonius, Delft and MacScience, Japan). Non-hydrogen atoms were refined anisotropically. Hydrogen atoms were located geometrically and were refined isotropically.

#### 4.2.1. Compound ***4a***

For X-ray crystallographic studies, compound **4a** was recrystallized as prismatic colorless crystals from n-butanol. Chemical formula $C_{20}H_{17}N_3O_3$, $M_r$ = 347.374, monoclinic, crystallizes in space group $P2_1/c$, Cell lengths "$a$ = 9.5834(2), $b$ = 7.7923(2), $c$ = 22.8262(8) Å", Cell angles "$\alpha$ = 90.00, $\beta$ = 96.1695(10), $\gamma$ = 90.00°", $V$ = 1694.71(8) Å$^3$, $Z$ = 4, $D_c$ = 1.362 mg/m$^3$, $\theta$ values 2.910–27.485°, absorption coefficient $\mu$ (Mo-$K_\alpha$) = 0.09 mm$^{-1}$, $F(000)$ = 728. The unique reflections measured 4045 of which 2349 reflections with threshold expression $I > 3\sigma(I)$ were used in the structural analysis. Convergence for 235 variable parameters by least-squares refinement on $F^2$ with $w = 1/[\sigma^2(F_o^2) + 0.10000\,F_o^2]$. The final agreement factors were R = 0.041 and $w$R = 0.077 with a goodness-of-fit of 1.019.

#### 4.2.2. Compound ***4m***

For X-ray crystallographic studies, compound **4m** was recrystallized as prismatic colorless crystals from n-butanol. Chemical formula $C_{21}H_{19}N_3O_4$, $M_r$ = 377.400, monoclinic, crystallizes in space group $P2_1/c$, Cell lengths "$a$ = 7.5625(3), $b$ = 18.7645(6), $c$ = 12.7045(6) Å", Cell angles "$\alpha$ = 90.00, $\beta$ = 94.6855(14), $\gamma$ = 90.00°", $V$ = 1796.83(12) Å$^3$, $Z$ = 4, $D_c$ = 1.395 mg/m$^3$, $\theta$ values 2.910–27.485°, absorption coefficient $\mu$ (Mo-$K_\alpha$) = 0.10 mm$^{-1}$, $F(000)$ = 792. The unique reflections measured 4670 of which 1865 reflections with threshold expression $I > 3\sigma(I)$ were used in the structural analysis. Convergence for 253 variable parameters by least-squares refinement on $F^2$ with $w = 1/[\sigma^2(F_o^2) + 0.10000\,F_o^2]$. The final agreement factors were R = 0.040 and $w$R = 0.072 with a goodness-of-fit of 1.151.

### 4.3. Anti-tumor activity screening

Anti-tumor properties of the synthesized compounds were screened by National Cancer Institute, Cairo University, Egypt, using the previously reported standard procedure adopting HCT116 (colon), MCF7 (breast) and HEPG2 (liver) human tumor cell lines [26]. Cells were seeded in 96-well microtiter plates at a concentration of $5 \times 10^4$–$10^5$ cell/well in a fresh medium and left for 24 h before treatment with the tested compounds to allow attachment of cells to the wall of the plate. The tested compounds were dissolved in dimethylsulfoxide (DMSO) and diluted 1000-fold in the assay. Different concentrations of the compounds under test (0, 5, 12.5, 25, and 50 $\mu$g/ml) were added to the cell monolayer. Triplicate wells were prepared for each individual dose. The monolayer cells were incubated with the tested compounds for 48 h at 37 °C, in atmosphere of 5% $CO_2$. After 48 h, the cells were fixed, washed and stained with Sulfo-Rhodamine-B (SRB) stain. Excess stain was washed with acetic acid. The attached stain was recovered with Tris–EDTA buffer. Cell survival and drug activity were determined by measuring the color intensity spectrophotometrically at 564 nm using an ELISA microplate reader (Meter tech. Σ 960, USA). Data are collected as mean values for experiments that performed in three replicates for each individual dose which measured by SRB assay. Control experiments did not exhibit significant change compared to the DMSO vehicle. Doxorubicin was used as a standard reference during the present in-vitro bioactivity screening assay. The percentage of cell survival was calculated as follows:

$$\text{Surviving fraction} = \text{Optical density(O.D.)of treated cells/O.D. of control cells} \quad (3)$$

The $IC_{50}$ (concentration required to produce 50% inhibition of cell growth compared to control experimental) was determined using Graph-Pad PRISM version-5 software. Statistical calculations for determination of the mean and standard error values were determined by SPSS 11 software. The observed anti-tumor properties were presented in Table 1 (Figs. 1–3 of the supplementary material).

## Acknowledgment

This work is sponsored by the Swedish International Development Cooperation Agency (SIDA) due to the International Collaborative Research Grant (MENA).

## Appendix. Supplementary data

Supplementary data related to this article can be found online at doi:10.1016/j.ejmech.2011.10.058. These data include MOL files and InChiKeys of the most important compounds described in this article.

## References


[1] (a) N.V. Lakshmi, Y. Arun, P.T. Perumal, Tetrahedron Lett. 52 (2011) 3437–3442;
(b) R. Prasanna, S. Purushothaman, M. Suresh, R. Raghunathan, Tetrahedron Lett. 52 (2011) 792–797;
(c) M.A. Ali, R. Ismail, T.S. Choon, Y.K. Yoon, A.C. Wei, S. Pandian, R.S. Kumar, H. Osman, E. Manogaran, Bioorg. Med. Chem. Lett. 20 (2010) 7064–7066;
(d) R. Rajesh, R. Raghunathan, Tetrahedron Lett. 51 (2010) 5845–5848;
(e) R. Prasanna, S. Purushothaman, R. Raghunathan, Tetrahedron Lett. 51 (2010) 4538–4542;
(f) K. Karthikeyan, P.M. Sivakumar, M. Doble, P.T. Perumal, Eur. J. Med. Chem. 45 (2010) 3446–3452;
(g) A. Hazra, P. Paira, K.B. Sahu, S. Naskar, P. Saha, R. Paira, S. Mondal, A. Maity, P. Luger, M. Weber, N.B. Mondal, S. Banerjee, Tetrahedron Lett. 51 (2010) 1585–1588;
(h) N.V. Lakshmi, P. Thirumurugan, P.T. Perumal, Tetrahedron Lett. 51 (2010) 1064–1068;
(i) R.S. Kumar, S.M. Rajesh, S. Perumal, D. Banerjee, P. Yogeeswari, D. Sriram, Eur. J. Med. Chem. 45 (2010) 411–422;
(j) S. Kathiravan, R. Raghunathan, Tetrahedron Lett. 50 (2009) 6116–6120;
(k) R.R. Kumar, S. Perumal, P. Senthilkumar, P. Yogeeswari, D. Sriram, Eur. J. Med. Chem. 44 (2009) 3821–3829;
(l) M. Ghandi, A. Yari, S.J.T. Rezaei, A. Taheri, Tetrahedron Lett. 50 (2009) 4724–4726;
(m) G. Periyasami, R. Raghunathan, G. Surendiran, N. Mathivanan, Eur. J. Med. Chem. 44 (2009) 959–966;
(n) R. Murugan, S. Anbazhagan, S.S. Narayanan, Eur. J. Med. Chem. 44 (2009) 3272–3279;
(o) A.R.S. Babu, R. Raghunathan, Tetrahedron Lett. 49 (2008) 4618–4620;
(p) P. Shanmugam, B. Viswambharan, K. Selvakumar, S. Madhavan, Tetrahedron Lett. 49 (2008) 2611–2615.
[2] C.B. Cui, H. Kakeya, H. Osada, Tetrahedron 52 (1996) 12651–12666.
[3] C.B. Cui, H. Kakeya, H. Osada, J. Antibiot. 49 (1996) 832–835.
[4] M.N.G. James, G.J.B. Williams, Can. J. Chem. 50 (1972) 2407–2412.
[5] A. Jossang, P. Jossang, H.A. Hadi, T. Sévenet, B. Bodo, J. Org. Chem. 56 (1991) 6527–6530.
[6] S. Ghosal, P.K. Banerjee, Indian J. Chem. 9 (1971) 289–293.
[7] K. Jones, J. Wilkinson, J. Chem. Soc. Chem. Commun. (1992) 1767–1769.
[8] S.I. Bascop, J. Sapi, J.Y. Laronze, J. Lévy, Heterocycles 38 (1994) 725–732.
[9] C. Pellegrini, C. Strässler, M. Weber, H.J. Borschberg, Tetrahedron: Asymmetry 5 (1994) 1979–1992.
[10] G. Palmisano, R. Annunziata, G. Papeo, M. Sisti, Tetrahedron: Asymmetry 7 (1996) 1–4.
[11] E. Garcia Prado, M.D. Garcia Gimenez, R. De la Puerta Vázquez, J.L. Espartero Sánchez, M.T. Sáenz Rodriguez, Phytomedicine 14 (2007) 280–284.
[12] R.D. Connell, Expert Opin. Ther. Pat. 13 (2003) 738–750.
[13] M.A. Jianguo, L.I. Shaolan, K. Reed, P. Guo, J.M. Gallo, J. Pharmacol. Exp. Ther. 305 (2003) 833–839.
[14] P. Marzola, A. Degrassi, L. Calderan, P. Farace, C. Crescimanno, E. Nicolato, A. Giusti, E. Pesenti, A. Terron, A. Sbarbati, T. Abrams, L. Murray, F. Osculati, Clin. Cancer Res. 15 (2004) 739–750.
[15] M.E. Lane, B. Yu, A. Rice, K.E. Lipson, C. Liang, L. Sun, C. Tang, G. McMahon, R.G. Pestell, S. Wadler, Cancer Res. 15 (2001) 6170–6177.
[16] A.H. Abadi, S.M. Abou-Seri, D.E. Abdel-Rahman, C. Klein, O. Lozach, L. Meijer, Eur. J. Med. Chem. 41 (2006) 296–305.
[17] (a) R. Grigg, S. Thianpatanagul, J. Chem. Soc. Chem. Commun. (1984) 180–181;
(b) R. Grigg, M.F. Aly, V. Sridharan, S. Thianpatanagul, J. Chem. Soc. Chem. Commun. (1984) 182–183;
(c) H. Ardil, R. Grigg, V. Sridharan, S. Suerendrakumar, S. Thianpatanagul, S. Kanajan, J. Chem. Soc. Chem. Commun. (1986) 602–604;
(d) A.R.S. Babu, R. Raghunathan, G. Gayatri, G.N. Sastry, J. Heterocycl. Chem. 43 (2006) 1467–1472.
[18] A.S. Girgis, Eur. J. Med. Chem. 44 (2009) 91–100.
[19] A.S. Girgis, Eur. J. Med. Chem. 44 (2009) 1257–1264.
[20] M.J.S. Dewar, E.G. Zoebisch, E.F. Healy, J.J.P. Stewart, J. Am. Chem. Soc. 107 (1985) 3902–3909.
[21] J.J.P. Stewart, J. Comput. Chem. 10 (1989) 209–220.
[22] J.J.P. Stewart, J. Comput. Chem. 10 (1989) 221–264.
[23] P. Machado, P.T. Campos, G.R. Lima, F.A. Rosa, A.F. C. Flores, H.G. Bonacorso, N. Zanatta, M.A.P. Martins, J. Mol. Struct. 917 (2009) 176–182.
[24] C.P. Frizzo, M.R.B. Marzari, D.N. Moreira, P.T. Campos, N. Zanatta, H.G. Bonacorso, M.A.P. Martins, J. Mol. Struct. 981 (2010) 71–79.
[25] (a) A.S. Girgis, N.S.M. Ismail, H. Farag, Eur. J. Med. Chem. 46 (2011) 2397–2407;
(b) A.S. Girgis, H. Farag, N.S.M. Ismail, R.F. George, Eur. J. Med. Chem. 46 (2011) 4964–4969.
[26] (a) P. Skehan, R. Storeng, D. Scudiero, A. Monks, J. McMahon, D. Vistica, J.T. Warren, H. Bokesch, S. Kenney, M.R. Boyd, J. Natl. Cancer Inst. 82 (1990) 1107–1112;
(b) A.S. Girgis, H.M. Hosni, F.F. Barsoum, Bioorg. Med. Chem. 14 (2006) 4466–4476;
(c) A.R. Katritzky, A.S. Girgis, S. Slavov, S.R. Tala, I. Stoyanova-Slavova, Eur. J. Med. Chem. 45 (2010) 5183–5199.
[27] D. Barnum, J. Greene, A. Smellie, P. Sprague, J. Chem. Inf. Comput. Sci. 36 (1996) 563–571.
[28] A. Smellie, S.L. Teig, P. Towbin, J. Comput. Chem. 16 (1995) 171–187.
[29] Y. Kurogi, O.F. Güner, Curr. Med. Chem. 8 (2001) 1035–1055.
[30] M.O. Taha, A.M. Qandil, D.D. Zaki, M.A. Al Damen, Eur. J. Med. Chem. 40 (2005) 701–727.
[31] M.O. Taha, A.G. Al-Bakri, W.A. Zalloum, Bioorg. Med. Chem. Lett. 16 (2006) 5902–5906.
[32] M.O. Taha, Y. Bustanji, M.A.S. Al-Ghussein, M. Mohammad, H. Zalloum, I.M. Al-Masri, N. Atallah, J. Med. Chem. 51 (2008) 2062–2077.
[33] M.O. Taha, Y. Bustanji, A.G. Al-Bakri, A. Yousef, W.A. Zalloum, I.M. Al-Masri, N. Atallah, J. Mol. Graph. Model. 25 (2007) 870–884.
[34] R. Abu Khalaf, G. Abu Sheikha, Y. Bustanji, M.O. Taha, Eur. J. Med. Chem. 45 (2010) 1598–1617.
[35] I.M. Al-Masri, M.K. Mohammad, M.O. Taha, Chem. Med. Chem. 3 (2008) 1763–1779.
[36] H. Kubinyi, Quant. Struct.-Act. Relat. 13 (1994) 393–401.
[37] H. Kubinyi, Quant. Struct.-Act. Relat. 13 (1994) 285–294.
[38] P.R. Duchowicz, M.G. Vitale, E.A. Castro, J.C. Autino, G.P. Romanelli, D.O. Bennardi, Eur. J. Med. Chem. 43 (2008) 1593–1602.
[39] M.P. Cava, A.A. Deana, K. Muth, M.J. Mitchell, Org. Synth. 41 (1961) 93–95.
[40] W.R. Roderick, J. Amer. Chem. Soc. 79 (1957) 1710–1712.
[41] Q. Ahmed, T. Wagner-Jauregg, E. Pretsch, J. Seibl, Helv. Chim. Acta 56 (1973) 1646–1655.
[42] A. Altomare, G. Cascarano, C. Giacovazzo, A. Guagliardi, M.C. Burla, G. Polidori, M. Camalli, J. Appl. Cryst. 27 (1994) 435–436.
[43] S. Mackay, C.J. Gilmore, C. Edwards, N. Stewart, K. Shankland, maXus Computer Program for the Solution and Refinement of Crystal Structures. Bruker Nonius, The Netherlands, MacScience, Japan & The University of Glasgow, 1999.